

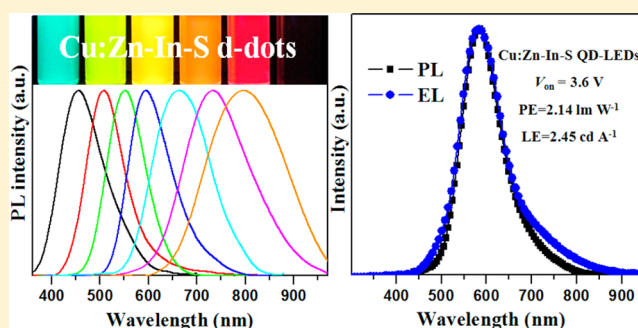
## Color-Tunable Highly Bright Photoluminescence of Cadmium-Free Cu-Doped Zn–In–S Nanocrystals and Electroluminescence

Wenjin Zhang,<sup>†</sup> Qing Lou,<sup>‡</sup> Wenyu Ji,<sup>‡</sup> Jialong Zhao,<sup>‡</sup> and Xinhua Zhong<sup>\*,†</sup><sup>†</sup>Shanghai Key Laboratory of Functional Materials Chemistry, Institute of Applied Chemistry, East China University of Science and Technology, Shanghai 200237, China<sup>‡</sup>State Key Laboratory of Luminescence and Applications, Changchun Institute of Optics, Fine Mechanics and Physics, Chinese Academy of Sciences, 3888 Eastern South Lake Road, Changchun 130033, China

## Supporting Information

**ABSTRACT:** A series of Cu doped Zn–In–S quantum dots (Cu:Zn–In–S d-dots) were synthesized via a one-pot noninjection synthetic approach by heating up a mixture of corresponding metal acetate salts and sulfur powder together with dodecanethiol in oleylamine media. After overcoating the ZnS shell around the Cu:Zn–In–S d-dot cores directly in the crude reaction solution, the resulting Cu:Zn–In–S/ZnS d-dots show composition-tunable photoluminescence (PL) emission over the entire visible spectral window and extending to the near-infrared spectral window (from 450 to 810 nm), with the highest PL quantum yield (QY) up to 85%. Importantly, the initial high PL QY of the obtained Cu:Zn–In–S/ZnS d-dots in organic media can be preserved when transferred into aqueous media via ligand exchange. Furthermore, electroluminescent devices with good performance (with a maximum luminance of 220 cd m<sup>-2</sup>, low turn-on voltages of 3.6 V) have been fabricated with the use of these Cd-free low toxicity yellow-emission Cu:Zn–In–S/ZnS d-dots as an active layer in these QD-based light-emitting diodes.

## KEYWORDS:



## INTRODUCTION

Colloidal luminescent semiconductor nanocrystals (NCs), also termed quantum dots (QDs), have been attracting increasing interest over the past two decades because of their unique optoelectronic properties and consequently in potential applications in the energy (photovoltaics and light emitting diodes, LED) and health (biomedical labeling and imaging) fields.<sup>1–7</sup> Initially, cadmium chalcogenide-based QDs (mainly CdS, CdSe, and CdTe) have been intensively investigated in the form of size- and composition-dependent photoluminescence (PL) tunable in the visible spectrum.<sup>8–15</sup> In QD-based light-emitting diodes (QD-LEDs), one of the most promising applications for QDs, the QD materials are also mainly focused on the CdSe-based NCs.<sup>16</sup> Despite their promising optoelectronic properties, the intrinsic toxicity of cadmium sheds doubt on the practical applicability of these QDs.<sup>2,3</sup> Therefore, exploring cadmium-free nanoemitters is urgent to meet the requirement of environmental friendliness in practical applications.

In recent years, cadmium-free doped quantum dots (d-dots) have been extensively studied since they possess not only the intrinsic advantages of QDs but also additional superiority such as improved thermal and chemical stability, a larger Stokes shift, a longer PL lifetime, etc.<sup>17–19</sup> Mn- and Cu-doped zinc chalcogenide d-dots are the most well-studied efficient emitters

among all the reported d-dots.<sup>20–49</sup> For Mn d-dots, the dopant emission wavelength is restricted within the yellow-orange spectral range (580–600 nm) since the dopant emission is originated from the intrinsic <sup>4</sup>T<sub>1</sub>–<sup>6</sup>A<sub>1</sub> transition of the Mn ion.<sup>20–40</sup> The Cu dopant emission could span over a much wider spectral range dependent on the nature, size, and composition of host NCs.<sup>39–49</sup> In previous reports, the PL emission in Cu d-dots is tuned in a wide wavelength range through varying the nature and particle size of binary NC hosts such as ZnS, ZnSe, CdS, and InP.<sup>39–45</sup> For example, Cu:ZnS d-dots show blue-green emission,<sup>39,41</sup> and Cu:ZnSe corresponds to green to yellow emission,<sup>40,42</sup> Cu:CdS to orange-red,<sup>43,44</sup> and Cu:InP to near-infrared.<sup>45</sup>

Besides binary II–VI and III–V compounds, semiconducting materials of ternary chalcogenide compounds AB<sub>m</sub>C<sub>n</sub> (A = Cu, Ag, Zn, Cd, etc.; B = Al, Ga, In; C = S, Se, Te) are promising alternatives to serve as doping hosts because they display composition-tunable electronic and optical properties.<sup>50,51</sup> The reported ternary chalcogenide compounds serving as host materials include Zn–Cd–S, ZnS/Zn–Cd–S, and Zn–In–Se systems.<sup>46–49</sup> For the Cu:Zn–Cd–S and Cu:ZnS/Zn–Cd–S d-dots,<sup>46–48</sup> even though high-quality PL emission over most of

Received: October 29, 2013

Published: December 19, 2013

the visible spectral window was obtained, high toxicity Cd is still present in these d-dots. For the Cd-free Cu:Zn–In–S system,<sup>49</sup> the obtained dopant emission wavelength range covers only 120 nm (from 540 to 660 nm) with an intermediate emission efficiency of 25–30%. Therefore, it is highly desirable to develop highly bright cadmium-free d-dots with a wide emission range to meet the versatile applications.

As a typical ternary chalcogenide material, Zn–In–S is a near-ideal candidate to serve as a doping host because of its high chemical stability, composition tunable optical band gaps, and well-developed synthetic method.<sup>52–54</sup> In previous reports, the Cu–Zn–In–S quaternary NCs have been synthesized as a NC emitter or photocatalyst for H<sub>2</sub> generation.<sup>55–58</sup> Herein, we report a new series of Cu doped Zn–In–S d-dots via a one-pot noninjection synthetic approach by heating up a mixture of corresponding metal acetate salts and sulfur powder together with dodecanethiol in oleylamine media. After overcoating the ZnS shell around the Cu:Zn–In–S cores directly in the crude reaction solution, the resultant Cu:Zn–In–S/ZnS d-dots show composition-tunable emission over the entire visible spectral window (from 450 to 810 nm) with the highest PL quantum yield (QY) up to 85%. Furthermore, we successfully carried out practical applications based on the obtained cadmium-free d-dots. The fabricated QD-LEDs based on the yellow-emission Cu:Zn–In–S/ZnS d-dots as an active layer displayed excellent optoelectronic performance.

## ■ EXPERIMENTAL SECTION

**Materials.** Zinc acetate (Zn(OAc)<sub>2</sub>, 99.99%), copper acetate (Cu(OAc)<sub>2</sub>, 99.99%), indium acetate (In(OAc)<sub>3</sub>, 99.99%), sulfur powder (99.99%), dodecanethiol (DDT, 99.9%), 11-mercaptoundecanoic acid (MUA, 95%), oleylamine (OAm, 97%), octadecene (ODE, 90%), and tetramethylammonium hydroxide (TMAH, 97%) were all obtained from Aldrich. All chemicals were used as received without further purification.

**Synthesis of Cu:Zn–In–S and Cu:Zn–In–S/ZnS d-Dots.** In a typical one-pot noninjection procedure, Cu(OAc)<sub>2</sub> (0.004 g, 0.02 mmol), Zn(OAc)<sub>2</sub> (0.037 g, 0.2 mmol), In(OAc)<sub>3</sub> (0.058 g, 0.2 mmol), and sulfur powder (0.051 g, 1.6 mmol) together with 4.0 mL of DDT and 6.0 mL of OAm were loaded in a 50-mL flask at room temperature. The mixture was heated to 220 °C at a heating rate of 15 °C/min under a nitrogen flow and kept at this temperature for a certain period of time to allow the growth of Cu:Zn–In–S d-dots. Aliquots of the sample were taken at different time intervals and injected into toluene solvent for recording of their optical spectra. After the completion of particle growth (usually 10 min), the reaction mixture was cooled to 60 °C, and 10 mL of toluene was added thereafter. The obtained Cu:Zn–In–S d-dots were precipitated by adding methanol into the toluene solution and purified by repeated centrifugation and decantation. To obtain Cu:Zn–In–S d-dots with different Zn/In ratios, the Zn/In precursor ratio was varied while the gross amount of Zn and In precursors and all other variables remained constant.

Deposition of the ZnS shell around the Cu:Zn–In–S core template was carried out in the crude Cu:Zn–In–S reaction mixture with a growth time of 10 min. First, the temperature of the reaction system was cooled to 100 °C; the Zn precursor (obtained by dissolving 0.4 mmol of Zn(OAc)<sub>2</sub> in 0.1 mL of OAm and 0.9 mL of ODE) was then introduced into the reaction mixture. Following this, the system temperature was raised to 240 °C with a heating rate of 15 °C/min and kept at this temperature for 20 min to allow the overgrowth of the ZnS shell around the preformed Cu:Zn–In–S core d-dots. Purification of Cu:Zn–In–S/ZnS was similar to that of Cu:Zn–In–S d-dots as described above. Water solubilization of the initially oil-soluble Cu:Zn–In–S/ZnS d-dots was carried out by replacing the initial hydrophobic surfactants with hydrophilic ligand MUA according to literature methods.<sup>59</sup>

**Characterization.** UV–vis spectra were monitored on a Shimadzu UV-2450 UV–vis. PL spectra were recorded on a Cary Eclipse (Varian) fluorescence spectrophotometer. The room temperature PL QYs of d-dots were calculated by the integrated emission of the d-dots samples in solution compared with that of rhodamine 6G with a PL QY of 95% in ethanol with identical optical density.<sup>13,60</sup> The PL lifetime study was performed with an Edinburgh FL 900 single-photon counting system equipped with a hydrogen lamp as the excitation source. The luminescence time range was selected at 0–5000 ns. Transmission electron microscopy (TEM) images were acquired using a JEOL JEM-2010 transmission electron microscope operating at an acceleration voltage of 200 kV. The TEM samples were obtained by depositing a drop of NC dispersion in toluene onto copper grids with carbon support. Powder X-ray diffraction (XRD) spectra were obtained using wide-angle X-ray diffraction on a Siemens D5005 X-ray powder diffractometer equipped with a graphite-monochromatized Cu K $\alpha$  radiation ( $\lambda = 1.5406$  Å). XRD samples were prepared by depositing NC powder on a piece of Si (100) wafer. The composition for the samples was measured by means of inductively coupled plasma atomic emission spectroscopy (ICP-AES, Thermo Elemental IRIS 1000). The samples were prepared by dissolving in HCl/HNO<sub>3</sub> (7/3, v/v). The electroluminescence (EL) spectra and current–voltage–luminance characteristics were measured using a Minolta Luminance Meter LS-110 and a programmable Keithley model 2400 power supply in the air at room temperature, respectively.

**Electroluminescent Device Fabrication.** All the devices were fabricated on indium tin oxide (ITO) coated glass substrates (15  $\Omega$ /square), which underwent an ultrasonic clean and UV-ozone treatment following standard literature procedures.<sup>61</sup> A layer of poly(3,4-ethylenedioxythiophene)/poly(styrenesulfonate) (PEDOT:PSS) was spin-coated onto the cleaned ITO substrate at 120 °C, followed by spin-coating a layer of poly(N,N'-bis(4-butylphenyl)-N,N'-bis(phenyl)benzidine (poly-TPD) at 110 °C. The d-dots dispersion in toluene (with OD value of 2) was then spin-coated on top of the poly-TPD. 1,3,5-Tris(N-phenylbenzimidazol-2-yl) benzene (TPBI) as the electron transport layer (ETL) was deposited by thermal evaporation at a pressure below  $4 \times 10^{-6}$  Torr. The electron injection layer (EIL), LiF, and the Al cathode were also deposited by thermal evaporation under the same conditions. The layer thickness and the deposition rate of the materials were monitored in situ using an oscillating quartz thickness monitor, and the deposition rates of TPBI and LiF were controlled to about 0.2 nm s<sup>-1</sup> and 0.01 nm s<sup>-1</sup>, respectively. The deposition rate of metal Al film was controlled at about 0.5 nm s<sup>-1</sup>.

## ■ RESULTS AND DISCUSSION

**Synthesis and Optical Properties of Cu:Zn–In–S and Cu:Zn–In–S/ZnS d-Dots.** The Cu:Zn–In–S d-dots were synthesized based on heating up a mixture of corresponding metal acetate salts, elemental sulfur together with DDT in OAm media, which were all loaded into a reaction flask at room temperature, via a one-pot noninjection synthetic approach. This facile noninjection method features high reproducibility and scale-up capability.<sup>15</sup> We choose the synthesis of Cu:Zn–In–S d-dots with an emission wavelength around 552 nm under a nominal Cu/Zn/In ratio of 1:10:10 as an example to demonstrate this one-pot noninjection approach in preparation of high-quality Cu doped alloyed NCs, and the detailed procedures are described in the Experimental Section. The Cu dopant emission evolved and intensified with the reaction time, and the highest PL QY could reach about 63% at a growth time of 10 min. Further injection of the Zn precursor to the preformed Cu:Zn–In–S d-dots reaction mixture system with the presence of an excess amount of sulfur precursor led to the formation of a Cu:Zn–In–S/ZnS core/shell nanostructure, and the corresponding PL QY was improved to more than 80%. To the best of our knowledge, this result is the highest one in

transition-metal-doped NCs and also among the best results in luminescent semiconductor nanocrystals.<sup>8–15,20–49</sup>

Temporal evolution of optical spectra (UV-vis absorption and PL emission spectra) of the resulting Cu:Zn–In–S dots synthesized under a nominal Cu/Zn/In precursor ratio of 1:10:10 with a growth temperature of 220 °C is shown in Figure 1. The poorly resolved excitonic absorption feature as

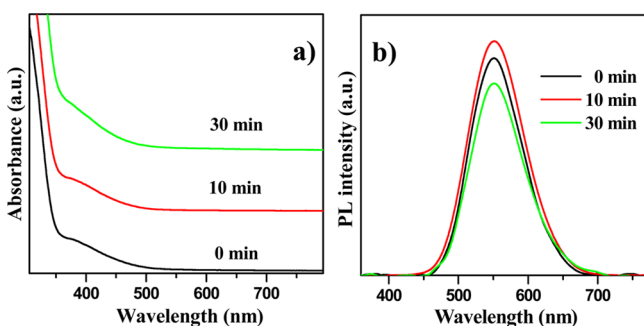


**Figure 1.** Temporal evolution of optical spectra of Cu:Zn–In–S d-dots dispersions in toluene prepared under a nominal Zn/In/Cu precursor molar ratio of 10:10:1 with a growth temperature of 220 °C. (a) UV-vis absorption and (b) PL emission ( $\lambda_{\text{ex}} = 350$  nm) spectra.

shown in Figure 1a is characteristic of ternary and quaternary alloyed NCs.<sup>11,59,61</sup> This may not mainly be caused by the wide size distribution because the special inhomogeneous composition distribution among different NCs in an ensemble can also be one of the reasons, which also influences the electronic properties.<sup>62</sup> The profile of absorption spectra (both the peak position and shape) bears almost no change within the whole growth period, which indicates that the particle size and chemical composition of the resulting NCs are kept constant. Figure 1b shows the corresponding PL emission spectra. The PL peak position also has no change during the whole growth period. This indicates a fast nucleation and growth process under specific reaction conditions. On the other hand, the PL QY in the beginning stage is very good, and the highest PL QY of 63% was observed at a growth time of 10 min. After then, the PL intensity decreased gradually along with the extension of growth time, and precipitation within the reaction mixture occurred with overextending the heating time (>30 min). The occurrence of precipitation may derive from the pyrolysis of the capping ligand DDT at high temperatures with overextending the heating time, which results in the destabilization and aggregation of the formed nanoparticles.

Although the as-prepared Cu:Zn–In–S d-dots have a high PL QY (up to 63%), but the PL of the as-prepared Cu:Zn–In–S d-dots is not stable enough to tolerate a harsh solution environment, especially in aqueous media. Previous reports have demonstrated that surface passivation of NCs using suitable inorganic materials with a higher band gap is an effect route to improve the PL QY and stability of NCs. For surface passivation, ZnS is a near-ideal selection for the construction of a core/shell nanostructure around the Cu:Zn–In–S d-dots due to its chemical stability, nontoxic characteristics, and large bulk band gap ( $E_{\text{g}} = 3.6$  eV) to localize the charge carriers inside the core region. The Cu:Zn–In–S/ZnS core/shell structure was constructed *in situ* from the crude Cu:Zn–In–S d-dots reaction solution with a growth time of 10 min. Due to the existence of an excess amount of a sulfur source in the reaction mixture, no additional sulfur source was necessary in the ZnS shell

overcoating process. To avoid separate nucleation of ZnS material, a Zn precursor ( $\text{Zn}(\text{OAc})_2$ ) was introduced into the reaction system at a lower temperature (100 °C), then the temperature of the reaction system was raised to 240 °C for the overgrowth of the ZnS shell around the Cu:Zn–In–S core template.

Figure 2 shows the evolution of optical spectra of Cu:Zn–In–S/ZnS core/shell NCs starting from the Cu:Zn–In–S d-

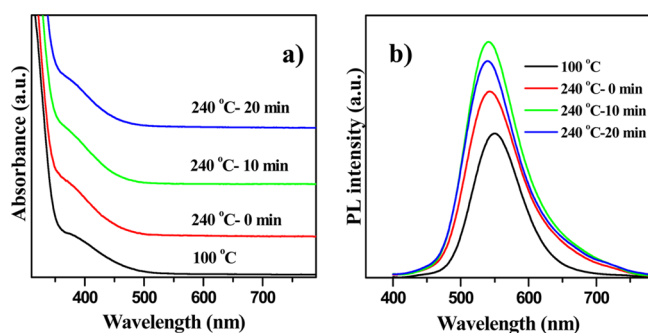


**Figure 2.** Temporal evolution of optical spectra of Cu:Zn–In–S/ZnS d-dots. (a) UV-vis absorption and (b) PL emission ( $\lambda_{\text{ex}} = 350$  nm) spectra.

dot cores with an emission wavelength of 550 nm prepared under the Cu/Zn/In precursor ratio of 1:10:10. With the overgrowth of the ZnS shell around the Cu:Zn–In–S core nanostructure, the PL peak position blue-shifted slightly from the initial 550 to 540 nm, and the corresponding PL QY increased substantially (from 63% to 85%). This PL QY is among the highest reported values for d-dots to date,<sup>20–49</sup> which paves a way for the use of Cu:Zn–In–S/ZnS NCs in many practical applications such as LED or fluorescent biological labeling and sensing. The small blue-shift of the PL peak position in the ZnS overcoating process indicates further incorporation of the zinc component into the core material, resulting in an increase of the band gap energy. A similar result was also observed in the  $\text{CuInS}_2/\text{ZnS}$  system.<sup>59,63</sup> It should be noted that the formation of the ZnS shell around the Cu:Zn–In–S d-dots accompanied with a small blue shift (about 10 nm) in the optical spectra is different from the previous report,<sup>49</sup> where a significant blue-shift (more than 80 nm) was observed when the Zn precursor was added into the Cu:Zn–In–S reaction solution at a high temperature. This significant blue-shift is ascribed to the ion exchange but not the formation of an extra shell layer in this report.<sup>49</sup>

To confirm that the enhancement of PL QY is due to overgrowth of the ZnS shell but not to further incorporation of the Cu component, we measured the Cu/In ratios before and after the ZnS shell deposition by ICP-AES. Experimental results show that the Cu/In ratios were kept almost constant before and after ZnS shell deposition (1:48.5, and 1:49.3, respectively). This result confirms our assumption that the enhancement of PL QY for the final d-dots is derived from the deposition of the ZnS shell around the Cu:Zn–In–S d-dots but not from the further incorporation of dopant Cu composition. In addition, the ZnS shell was also deposited successfully around Cu:Zn–In–S d-dot cores with the emission wavelength ranging from 450 to 770 nm corresponding to different Zn/In ratios, and the corresponding emission peak wavelength of the resulting Cu:Zn–In–S/ZnS tunable from 450 to 810 nm. The detailed PL spectra of Cu:Zn–In–S/ZnS before and after ZnS

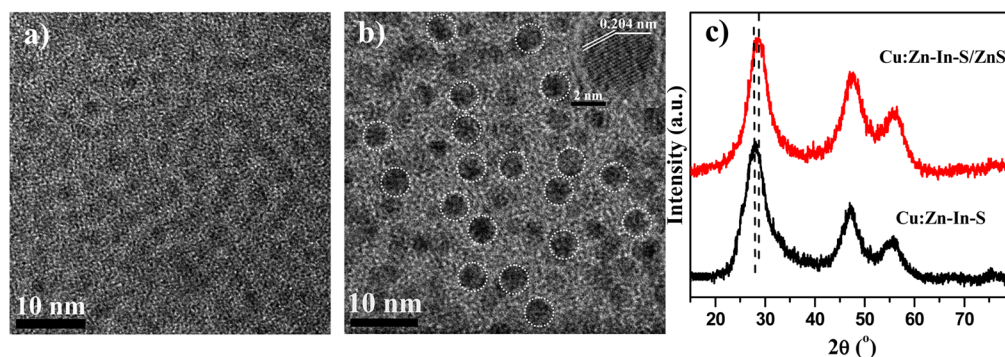


**Figure 3.** Wide-field TEM images of a Cu:Zn–In–S d-dots sample with a growth time of 10 min (a) and the derivate Cu:Zn–In–S/ZnS d-dots (b). (c) XRD patterns of the samples as shown in a and b.

shell deposition are shown in Figure S1 in the Supporting Information (SI).

**Morphology and Structure of the Cu:Zn–In–S and Cu:Zn–In–S/ZnS d-Dots.** Morphology and structural characterization of Cu:Zn–In–S and Cu:Zn–In–S/ZnS d-dots were performed with the use of TEM and XRD. The TEM images (Figure 3a) demonstrate that all of the as-obtained NCs are of near-spherical shape and possess high size uniformity. Figure 3a,b show that the average diameter of the Cu:Zn–In–S and Cu:Zn–In–S/ZnS d-dots was determined to be  $2.4 \pm 0.3$  nm and  $3.9 \pm 0.3$  nm, respectively, which indicates that about two monolayers of ZnS shell are overcoated around the Cu:Zn–In–S core. The histograms of size distribution for Cu:Zn–In–S and Cu:Zn–In–S/ZnS d-dots based on the statistic analysis of more than 200 particles are given in Figure S2 of the Supporting Information (SI). The lattice spacing of 0.204 nm as shown in the inset of Figure 3b should be ascribed to the (102) planes of zinc blende Zn–In–S crystals. The wide-angle XRD patterns (Figure 3c) of the obtained d-dots showed the characteristic peaks of the zinc blende (cubic) structure of the obtained NCs. When the ZnS shell was overcoated around the Cu:Zn–In–S core, the pattern of the cubic lattice was maintained in the core/shell structures, but the diffraction peaks shifted to larger angles. This observation is consistent with the smaller lattice constant for ZnS compared with Zn–In–S. No diffraction peaks from Cu impurities were detected in the samples. In addition, we can conclude that doping Cu into the host alloyed NCs does not bring about a phase transformation of the crystal structure.

**Dopant Emission.** Even though the observed wide PL emission wavelength range (from 450 to 810 nm) in our Cu:Zn–In–S d-dots can undoubtedly exclude the possibility of PL originating from the band edge emission, there is still the possibility to ascribe the PL to the surface trap emission, which also meets the peak position and broad nature of the claimed Cu dopant emission. To explore the origin of the observed PL emission, control experiments were carried out. First, Zn–In–S alloyed NCs without the presence of Cu composition were synthesized. The absorption pattern for the samples with the absence of a small amount of Cu is similar to that with the presence of Cu, but no PL emission was observed in the case of absence of Cu (corresponding optical spectra available in Figure S3). For the case with an absence of any one of In, Zn, or S, neither such absorption nor emission was observed. This indicates that host NCs are composed of an alloy of In and Zn, and the formed alloy host determines the absorption edge,

while the Cu component only serves as a dopant and takes the responsibility for PL emission in the composite NC system.

To determine furthermore that the PL emission originates from the Cu dopant, we carried out a transient PL decay dynamic study. It is reported that a size-dependent band gap and intrinsic and surface defects of NCs are all contributors to the PL emission, but different charge carrier recombination pathways correspond to different PL decay lifetimes.<sup>64</sup> This offers the possibility to distinguish the dopant emission from the trap emission in our studied d-dots. According to the literature data, PL lifetimes of the excitonic emission as well as the surface trap emission of QDs are in the range of a few and tens of nanoseconds,<sup>65–68</sup> whereas the corresponding lifetime for dopant emission in doped NCs is expected to be as long as hundreds of nanoseconds.<sup>32,59</sup> We performed the measurement of the decay curves of the PL emission with representative emission wavelengths of 450, 552, 630, and 710 nm from the Cu:Zn–In–S samples with corresponding In/Zn ratios of 0.31, 0.86, 2.8, and 16.6, respectively. Herein, the room temperature PL decay time (i.e., the excited state lifetimes,  $\tau_{1/e}$ ), at which the PL intensity has decreased to  $1/e$  of its initial value, is used as a parameter to compare the lifetimes. We observed the PL excited-state lifetime located in the range of 103–453 ns, and it was enhanced with an increase of the In ratio in the alloyed host NCs (Figure 4). This observed hundreds of nanoseconds PL lifetime confirms the emission originated from the Cu dopant transition but not from surface states of host NCs.

**Influence of Experimental Variables on the Optical Properties of Cu:Zn–In–S d-Dots.** The PL features (PL peak position and PL intensity) of the resulting Cu:Zn–In–S d-dots were found to be heavily dependent on the experimental

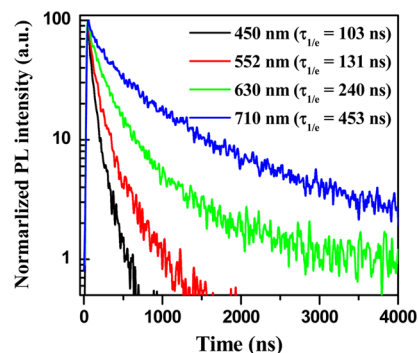


**Figure 4.** PL decay curves of Cu:Zn–In–S d-dots with typical emission wavelengths.

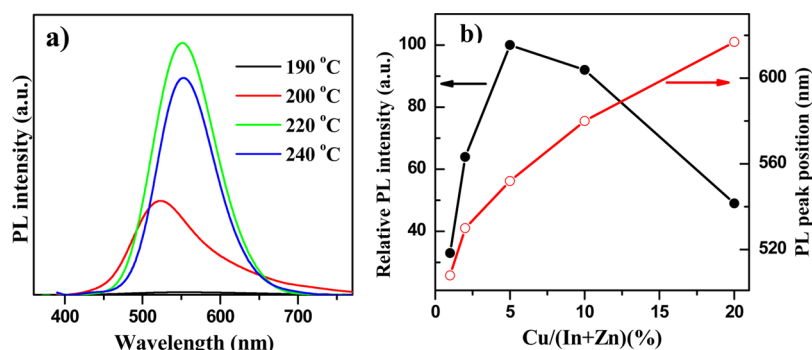


**Figure 5.** Influence of experimental variables on the PL properties of Cu:Zn–In–S d-dots. (a) PL spectra under different growth temperatures. (b) Summarization of the dependence of relative PL intensity and peak position on the Cu/(Zn+In) ratio.

variables such as the reaction temperature, the molar ratios of Cu:(Zn+In), Zn/In, and the amounts of elementary sulfur and DDT. In the investigation of the influence of different experimental variables on the optical properties of the obtained d-dots, we fixed all the other experimental variables as stated in the Experimental Section and varied the studied variable only.

**Influence of Reaction Temperature.** Reaction temperature is a crucial factor in determining the whole doping process, which includes surface adsorption/desorption, lattice incorporation/ejection, lattice diffusion, etc.<sup>28,47</sup> Therefore, an appropriate temperature is critical to determining the formation of high-quality d-dots. Experimental results indicate that absorption spectra do not show an obvious dependence on the reaction temperature in the studied range (from 190 to 240 °C) as shown in Figure S4, while the situation of the PL feature is completely different (Figure 5a). It is found that when the reaction temperature was lower than 190 °C, no dopant PL emission could be observed. This may be ascribed to the failure of incorporation of the dopant Cu component into the host lattice to act as a recombination center due to the low temperature.<sup>28</sup> With the increase of the reaction temperature from 190 to 200 °C, the dopant PL intensity increased sharply. This indicates that the Cu component is beginning to incorporate into the host crystal lattice to show a dopant PL emission. Therefore, this abrupt enhancement of PL intensity can be attributed to the transition of the “dopant lattice adsorption” process to the “dopant lattice diffusion” one as described by Peng et al.<sup>28</sup> On the other hand, we can deduce that the “lattice diffusion” temperature for the Cu:Zn–In–S d-dots system would be about 205–215 °C. When the temperature was raised to more than 240 °C, the PL intensity started to decrease, and precipitation of the NCs within the reaction mixture occurred. The observed precipitation can be attributed to the fact that DDT acts both as the sulfur precursor and as the stabilizing ligand in the reaction system. Therefore, its gradual decomposition at high temperatures results in a destabilization and aggregation of the colloidal particles.

**Effect of Dopant Concentration.** According to previous reports, the PL features of d-dots have a heavy dependence on the dopant concentration.<sup>18,27,39,40</sup> In the dopant concentration experiment, a series of Cu:Zn–In–S d-dot samples with different nominal Cu/(In + Zn) ratios (1–20%) were synthesized. As shown in Figure S5, the absorption spectra of Cu:Zn–In–S d-dots under Cu/(Zn+In) ratios of 1–5% showed an almost identical spectral profile. This indicates that when the dopant concentration is at a low level (<5%), the size and composition of the host Zn–In–S NCs do not depend

on the concentration of dopant Cu. However, the absorption spectra showed a systematic red-shift with an increase of the dopant Cu amount when the ratio was above 10%. In comparison, the PL intensity and peak position in the PL emission spectra of the resulting Cu:Zn–In–S d-dots also showed a substantial dependence on the Cu precursor contents, and this dependence was summarized in Figure 5b. The PL emission peak shifted from 518 to 606 nm monotonously with increasing the Cu content from 1% to 20%. With the increase of Cu/(In + Zn) ratio from 1% to 5%, the PL intensity increased rapidly, and that showed a maximum value at about 5% Cu concentration. With a further increase of Cu content, the PL intensity decreased gradually. Besides the Cu content, the optimal amounts for DDT and sulfur were also explored. It was found that the highest PL QY was obtained under conditions of 4.0 mL of DDT and 1.6 mmol of sulfur.

**Composition-Dependent Emission Color Tunable from Blue to NIR.** Previous reports have proved that Cu ion doping emission derived from the recombination of electrons in the conduction band of the host material and holes in the Cu T<sub>2</sub> state.<sup>46</sup> Therefore, we can tune the Cu ion dopant emission wavelength by varying the size and/or composition of alloyed host materials as done in previous reports.<sup>39–49</sup> Size-tuning was the mainstream to vary the band gap of NCs in the previous literature.<sup>39–45</sup> However, size-tuning may cause problems in many applications, in particular, if unstable small particles (less than 2 nm) are used. Recently, a few research groups focused on composition-dependent band gap tuning in alloy NCs, and great success has been achieved.<sup>46–49</sup> For example, we have synthesized Cu doped Zn<sub>x</sub>Cd<sub>1-x</sub>S d-dots with superior PL QY (from 30% to 65%) and wide PL range (from 450 to 710 nm) via controlling the stoichiometric ratio of Zn/Cd in the resulting d-dots.<sup>47</sup>

In the experiments, the nominal In/Zn precursor molar ratio was varied from 0.33:1 to 19:1 with fixation of the gross amount of In and Zn precursors at 0.4 mmol. The chemical compositions of the resulting Cu:Zn–In–S d-dot samples were determined by ICP-AES measurement (listed in Table S1). Based on the ICP data, the In/Zn atomic ratios were calculated and compared with the nominal values. It can be found that the real In/Zn ratios in the final samples are a little bit lower than those of the nominal values. This may be due to the different chemical reactivity of In and Zn precursors. Experimental results show that, with the increase of the nominal In/Zn precursor ratio from 0.33:1 to 19:1, the first excitonic absorption peak of Zn–In–S alloyed NCs red-shifted systematically from 376 to 513 nm (Figure S6a). As expected, the

corresponding Cu dopant emission also red-shifted, but at a much more pronounced extent from 450 to 710 nm (Figure S6b). It should be noted that the particle size remained almost constant with the variation of the In/Zn precursor ratio. These features of fixation of particle size and the red-shift of excitonic absorption peak give strong evidence to confirm the alloy structure of the host Zn–In–S NCs. Figure 6 summarizes the

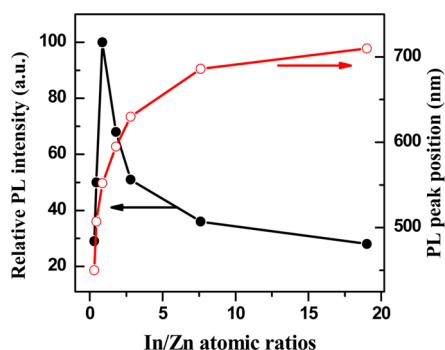


**Figure 6.** Summarization of the dependence of relative PL intensity and peak position of the Cu:Zn–In–S d-dots on the In/Zn ratio in the final samples.

dependence of PL intensity and PL peak position of the dopant emission in the resulting Cu:Zn–In–S d-dots on the In/Zn ratio in the final samples. In principle, with an increase of the In/Zn ratio from 0.31:1 to 16.6:1, the PL intensity increased rapidly and approached the highest value (with ~63% PL QY) at an In/Zn ratio of 0.86:1. Then, the PL intensity reduced systematically with a further increase of the In/Zn ratio. The deep red emission from the obtained Cu:Zn–In–S samples can rule out the possibility of the PL originating from the band edge emission from host Zn–In–S NCs, since the bulk band gaps of  $\text{In}_2\text{S}_3$  and ZnS are 2.1 eV (606 nm) and 3.7 eV (335 nm), respectively. As for the explanation of the observed remarkable red-shift (from 450 to 710 nm) of Cu dopant emission with the increase of In/Zn ratio, it can be ascribed to the well-known fact that the band gap of the alloyed NCs decreases accordingly with the increase of content of low band gap  $\text{In}_2\text{S}_3$  in the Zn–In–S alloyed NCs. Because of the much smaller electron effective mass versus the significantly larger hole mass, most of the band gap decrease is seen as a shift in the conduction band edge to lesser negative potentials; thus, it results in lowering down of the Cu dopant emission, which is derived from the

recombination of the electron in the conduction band of the host material and hole in the Cu  $T_2$  state.

As shown in Figure 7a, the emission wavelength of the obtained Cu:Zn–In–S/ZnS NCs with different In/Zn ratios can cover the entire visible and partial near-infrared window (from 450 to 810 nm). A digital picture of the Cu:Zn–In–S/ZnS samples with different emissive wavelengths under UV irradiation is shown in Figure 7b. The best PL QY of the dopant emission at 540 nm has been observed to be 85%, and the average value is in the range of 70–80%. Therefore, the obtained Cu dopant NCs could be a potential color tunable dispersed NC emitter in applications such as LED, lasers, and biomedical fluorescent labels.

**Highly Stability of QDs.** The as-prepared Cu:Zn–In–S/ZnS d-dots were transferred into an aqueous solution through ligand exchange by MUA. Both the position of the first absorption peak and the shape of absorption spectra did not undergo observable variation in the process of ligand exchange, as shown in Figure 8a. PL intensity of the resultant water-

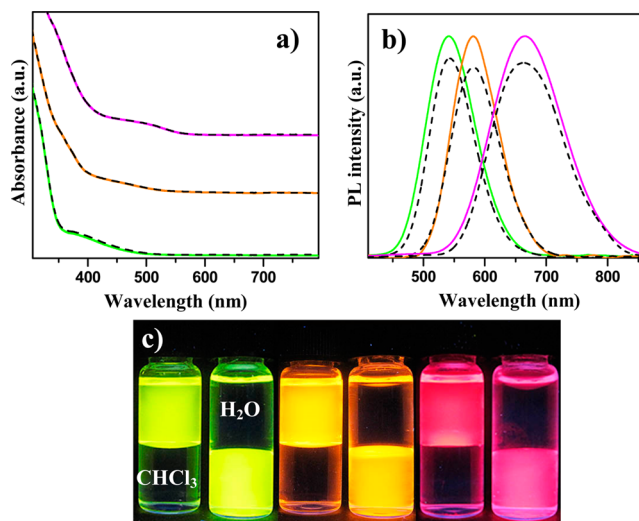


**Figure 8.** UV spectra (a) and PL spectra (b) of Cu:Zn–In–S/ZnS samples before ( $\text{CHCl}_3$  dispersions) and after (aqueous dispersions) phase transfer using MUA. (c) Photographs of samples dispersed in different media under UV illumination.

soluble d-dots is only slightly decreased (about 10–15%) compared to that of the initial oil-soluble samples (Figure 8b). Figure 8c shows the luminescence photographs of three

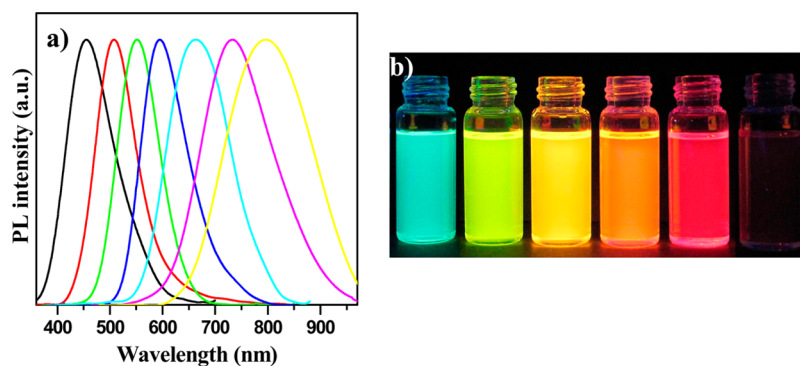


**Figure 7.** (a) Normalized PL emission spectra ( $\lambda_{\text{ex}} = 350$  nm) of Cu:Zn–In–S/ZnS d-dots under different In/Zn precursor ratios and Cu ion concentration. (b) Digital picture of samples under the radiation of a UV lamp.

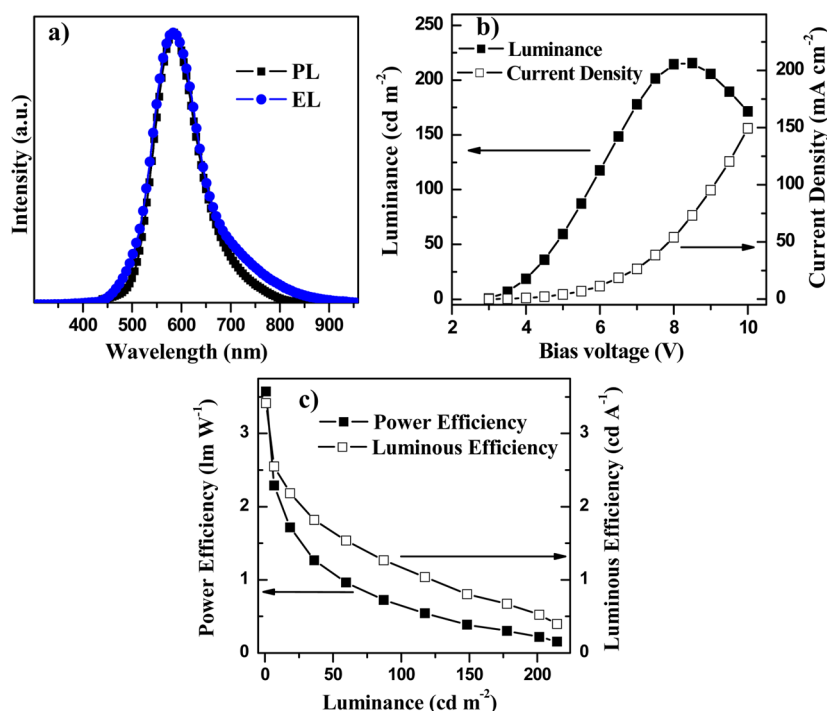


**Figure 9.** (a) The PL spectra and corresponding EL of Cu doped Zn–In–S/ZnS with yellow color. (b) Current density and luminance of the devices with yellow emission colors as a function of applied bias. (c) Current efficiency and power efficiency of yellow devices as a function of current density.

representative Cu:Zn–In–S/ZnS d-dots with green, yellow, and red emission colors to demonstrate the bright luminescence in both a polar solvent and aqueous solution under UV illumination.

We also have simply checked the thermal stability of d-dots through a digital picture of samples at different temperatures under the radiation of a UV lamp (Figure S7). The experimental results indicated that these Cu d-dots did not show a significant change in emissive intensity when heating up to 250 °C. These proved advantages further solidify their many applications such as light emitting devices.

**Practical Light-Emitting Application.** The CuInS<sub>2</sub>-based Cd-free QD-LEDs have been reported by a few groups and displayed excellent optoelectronic properties.<sup>69,70</sup> In our case, electroluminescent devices have also been fabricated with the use of the above-reported Cd-free low toxicity Cu:Zn–In–S/ZnS QDs (yellow-emission with mission wavelength at 580 nm) as active layers in LEDs. The multilayer structure contains ITO/PEDOT:PSS (10 nm)/poly-TPD (40 nm)/d-dots/TPBI (40 nm)/LiF (0.5 nm)/Al (100 nm). The poly-TPD and TPBI layers were selected as the hole-transporting (HTL) and the electron-transporting (ETL) layers, respectively. More details of the device fabrication and characterization are described in the Experimental Section.

Figure 9a shows the normalized EL spectra and their corresponding PL spectra with an emission peak at 580 nm. The fwhm of the EL emission was broader in comparison with that of corresponding PL spectra. This indicates that the device emissions are mainly derived from the Cu doped Zn–In–S/ZnS d-dots. The measured luminance–current–voltage ( $L$ – $I$ – $V$ ) characteristics of the LED devices are shown in Figure 9b. The turn-on voltages ( $V_{on}$ ) is only 3.6 V, which is lower than that of the reported lowest value for CuInS<sub>2</sub> based QD-LED (4.4 V).<sup>69</sup> The maximum QD-LEDs luminance reached 220 cd

m<sup>-2</sup> (at 8.5 V). The luminous efficiency and power efficiency of the fabricated devices were also calculated. A luminous efficiency (LE) of 2.45 cd A<sup>-1</sup> and a power efficiency (PE) of 2.14 lm W<sup>-1</sup>, at an injection current density of 0.41 mA cm<sup>-2</sup>, corresponding to a brightness of 10 cd m<sup>-2</sup>, were observed for the LED, as seen in Figure 9c, which is also better compared to that (LE = 0.92 cd A<sup>-1</sup>, PE = 0.61 lm W<sup>-1</sup>, at an injection current density of 1.18 mA cm<sup>-2</sup>, corresponding to a brightness of 10 cd m<sup>-2</sup>) of CuInS<sub>2</sub>-based QD-LED.<sup>69,70</sup> Therefore, we think that the Cu doped Zn–In–S/ZnS d-dots can be potential outstanding Cd-free candidates to fabricate LEDs.

## CONCLUSION

High quality Cu doped Zn–In–S/ZnS d-dots with composition-tunable emission (from 450 to 810 nm) and a maximum PL QY of 85% have been synthesized using a one pot noninjection synthetic approach. Emission wavelengths covering from the visible spectrum to the near-infrared window can be facily tuned by the variation of the composition of Zn–In–S alloyed NCs under identical particle size. Importantly, the high PL QY of the initial oil-soluble d-dots can be preserved when transferred into aqueous media via ligand exchange. Moreover, the application of these cadmium-free d-dots was explored for use in light emitters for electroluminescent devices. The primary results demonstrated the promising potential of Cu:Zn–In–S/ZnS d-dots as alternative materials for LED applications, and the performance could be further improved by optimizing the materials and device structure. Overall, the reported Cu:Zn–In–S/ZnS d-dots have promising potential as less toxic NCs for applications in LEDs and biolabeling.

## ■ ASSOCIATED CONTENT

### Supporting Information

Optical properties of the NCs with different cores, under different growth temperatures, different Cu/(Zn+In) precursor ratios, and different In/Zn precursor ratios; the histograms of size distribution of NCs, absorption of Zn–In–S d-dots, nominal and real In/Zn atomic ratios in Cu:Zn–In–S d-dots. This material is available free of charge via the Internet at <http://pubs.acs.org>.

## ■ AUTHOR INFORMATION

### Corresponding Author

\*Fax: +86 21 6425 0281. E-mail: [zhongxh@ecust.edu.cn](mailto:zhongxh@ecust.edu.cn).

### Notes

The authors declare no competing financial interest.

## ■ ACKNOWLEDGMENTS

The work was supported by National Natural Science Foundation of China (No. 21175043), the Science and Technology Commission of Shanghai Municipality (11JC1403100, 12NM0504101, 12ZR1407700), and the Fundamental Research Funds for the Central Universities for financial support.

## ■ REFERENCES

- (1) Talapin, D. V.; Lee, J. S.; Kovalenko, M. V.; Shevchenko, E. V. *Chem. Rev.* **2010**, *110*, 389–458.
- (2) Zrazhevskiy, P.; Sena, M.; Gao, X. *Chem. Soc. Rev.* **2010**, *39*, 4326–4354.
- (3) Lohse, S. E.; Murphy, C. J. *J. Am. Chem. Soc.* **2012**, *134*, 15607–15620.
- (4) Kershaw, S. V.; Susha, A. S.; Rogach, A. L. *Chem. Soc. Rev.* **2013**, *42*, 3033–3087.
- (5) Wang, J.; Mora-Seró, I.; Pan, Z.; Zhao, K.; Zhang, H.; Feng, Y.; Yang, G.; Zhong, X.; Bisquert, J. *J. Am. Chem. Soc.* **2013**, *135*, 15913–15922.
- (6) Rogach, A. L.; Gaponik, N.; Lupton, J. M.; Bertoni, C.; Gallardo, D. E.; Dunn, S.; Pira, N. L.; Paderi, M.; Repetto, P.; Romanov, S. G.; O'Dwyer, C.; Torres, C. M. S.; Eychmuller, A. *Angew. Chem., Int. Ed.* **2008**, *47*, 6538–6549.
- (7) Nozik, A. J.; Beard, M. C.; Luther, J. M.; Law, M.; Ellingson, R. J.; Johnson, J. C. *Chem. Rev.* **2010**, *110*, 6873–6890.
- (8) Murray, C. B.; Norris, D. J.; Bawendi, M. G. *J. Am. Chem. Soc.* **1993**, *115*, 8706–8715.
- (9) Peng, Z. A.; Peng, X. *J. Am. Chem. Soc.* **2001**, *123*, 183–184.
- (10) Qu, L.; Peng, X. *J. Am. Chem. Soc.* **2002**, *124*, 2049–2055.
- (11) Zhong, X.; Han, M.; Dong, Z.; White, T. J. *J. Am. Chem. Soc.* **2003**, *125*, 8589–8594.
- (12) Bae, W. K.; Char, K.; Hur, H.; Lee, S. *Chem. Mater.* **2008**, *20*, 531–539.
- (13) Donega, C. D. *Chem. Soc. Rev.* **2011**, *40*, 1512–1546.
- (14) Regulacio, M. D.; Han, M.-Y. *Acc. Chem. Res.* **2010**, *43*, 621–630.
- (15) Zhang, W.; Zhang, H.; Feng, Y.; Zhong, X. *ACS Nano* **2012**, *6*, 11066–11073.
- (16) Shirasaki, Y.; Supran, G. J.; Bawendi, M. G.; Bulović, V. *Nat. Photonics* **2013**, *7*, 13–23.
- (17) Peng, X. *Acc. Chem. Res.* **2010**, *43*, 1387–1395.
- (18) Norris, D. J.; Efros, A. L.; Erwin, S. C. *Science* **2008**, *319*, 1776–1779.
- (19) Erwin, S. C.; Zu, L.; Haftel, M. I.; Efros, A. L.; Kennedy, T. A.; Norris, D. J. *Nature* **2005**, *436*, 91–94.
- (20) Suyver, J. F.; Wuister, S. F.; Kelly, J. J.; Meijerink, A. *Nano Lett.* **2001**, *1*, 429–433.
- (21) Bol, A. A.; Meijerink, A. *J. Phys. Chem. B* **2001**, *105*, 10197–10202.
- (22) Norris, D. J.; Yao, N.; Charnock, F. T.; Kennedy, T. A. *Nano Lett.* **2001**, *1*, 3–7.
- (23) Pradhan, N.; Goorskey, D.; Thessing, J.; Peng, X. *J. Am. Chem. Soc.* **2005**, *127*, 17586–17587.
- (24) Yang, Y.; Chen, O.; Angerhofer, A.; Cao, Y. C. *J. Am. Chem. Soc.* **2006**, *128*, 12428–12429.
- (25) Pradhan, N.; Peng, X. *J. Am. Chem. Soc.* **2007**, *129*, 3339–3347.
- (26) Yang, Y.; Chen, O.; Angerhofer, A.; Cao, Y. C. *J. Am. Chem. Soc.* **2008**, *130*, 15649–15661.
- (27) Nag, A.; Chakraborty, S.; Sarma, D. D. *J. Am. Chem. Soc.* **2008**, *130*, 10605–10611.
- (28) Chen, D.; Viswanatha, R.; Ong, G. L.; Xie, R.; Balasubramanian, M.; Peng, X. *J. Am. Chem. Soc.* **2009**, *131*, 9333–9339.
- (29) Wang, C.; Gao, X.; Ma, Q.; Xu, X. *J. Mater. Chem.* **2009**, *19*, 7016–7022.
- (30) Zheng, J.; Yuan, X.; Ikezawa, M.; Jing, P.; Liu, X.; Zheng, Z.; Kong, X.; Zhao, J.; Masumoto, Y. *J. Phys. Chem. C* **2009**, *113*, 16969–16974.
- (31) Zheng, J.; Ji, W.; Wang, X.; Ikezawa, M.; Jing, P.; Liu, X.; Li, H.; Zhao, J.; Masumoto, Y. *J. Phys. Chem. C* **2010**, *114*, 15331–15336.
- (32) Fang, Z.; Wu, P.; Zhong, X.; Yang, Y. *J. Nanotechnology* **2010**, *21*, 305604.
- (33) Zeng, R.; Rutherford, M.; Xie, R.; Zou, B.; Peng, X. *Chem. Mater.* **2010**, *22*, 2107–2113.
- (34) Srivastava, B. B.; Jana, S.; Karan, N. S.; Paria, S.; Jana, N. R.; Sarma, D. D.; Pradhan, N. *J. Phys. Chem. Lett.* **2010**, *1*, 1454–1458.
- (35) Acharya, S.; Sarma, D. D.; Jana, N. R.; Pradhan, N. *J. Phys. Chem. Lett.* **2010**, *1*, 485–488.
- (36) Zhu, D.; Jiang, X.; Zhao, C.; Sun, X.; Zhang, J.; Zhu, J. *Chem. Commun.* **2010**, *46*, 5226–5228.
- (37) Zeng, R.; Zhang, T.; Dai, G.; Zou, B. *J. Phys. Chem. C* **2011**, *115*, 3005–3010.
- (38) Zhang, W.; Li, Y.; Zhang, H.; Zhou, X.; Zhong, X. *Inorg. Chem.* **2011**, *50*, 10432–10438.
- (39) Karan, N. S.; Sarma, D. D.; Kadam, R. M.; Pradhan, N. *J. Phys. Chem. Lett.* **2010**, *1*, 2863–2866.
- (40) Shen, H.; Wang, H.; Li, X.; Niu, J.; Wang, H.; Chen, X.; Li, L. *Dalton Trans.* **2009**, 10534–10540.
- (41) Corrado, C.; Hawker, M.; Livingston, G.; Medling, S.; Bridges, F.; Zhang, J. *Nanoscale* **2010**, *2*, 1213–1221.
- (42) Jana, S.; Srivastava, B. B.; Acharya, S.; Santra, P. K.; Jana, N. R.; Sarma, D. D.; Pradhan, N. *Chem. Commun.* **2010**, *46*, 2853–2855.
- (43) Mandal, P.; Talwar, S. S.; Major, S. S.; Srinivasa, R. S. *J. Chem. Phys.* **2008**, *128*, 114703/1–114703/7.
- (44) Stouwdam, J. W.; Janssen, R. A. J. *Adv. Mater.* **2009**, *21*, 2916–2920.
- (45) Xie, R.; Peng, X. *J. Am. Chem. Soc.* **2009**, *131*, 10645–10651.
- (46) Srivastava, B. B.; Jana, S.; Pradhan, N. *J. Am. Chem. Soc.* **2011**, *133*, 1007–1015.
- (47) Zhang, W.; Zhou, X.; Zhong, X. *Inorg. Chem.* **2012**, *51*, 3579–3587.
- (48) Chen, Y.; Huang, L.; Li, S.; Pan, D. *J. Mater. Chem. C* **2013**, *1*, 751–756.
- (49) Sarkar, S.; Karan, N. S.; Pradhan, N. *Angew. Chem., Int. Ed.* **2011**, *50*, 6065–6069.
- (50) Zhong, H.; Bai, Z.; Zou, B. *J. Phys. Chem. Lett.* **2012**, *3*, 3167–3175.
- (51) Omata, T.; Nose, K.; Otsuka-Yao-Matsuo, S. *J. Appl. Phys.* **2009**, *105*, 073106.
- (52) Gou, X.; Cheng, F.; Shi, Y.; Zhang, L.; Peng, S.; Chen, J.; Shen, P. *J. Am. Chem. Soc.* **2006**, *128*, 7222–7229.
- (53) Chen, Z.; Li, D.; Zhang, W.; Chen, C.; Li, W.; Sun, M.; He, Y.; Fu, X. *Inorg. Chem.* **2008**, *47*, 9766–9772.
- (54) Shen, S.; Zhao, L.; Guo, L. *Int. J. Hydrogen Energy* **2010**, *35*, 10148–10154.
- (55) Trizio, L. D.; Prato, M.; Genovese, A.; Casu, A.; Povia, M.; Simonutti, R.; Alcocer, M. J. P.; D'Andrea, C.; Tassone, F.; Manna, L. *Chem. Mater.* **2012**, *24*, 2400–2406.

- (56) Wu, T.; Zhang, Q.; Hou, Y.; Wang, L.; Mao, C.; Zheng, S.; Bu, X.; Feng, P. *J. Am. Chem. Soc.* **2013**, *135*, 10250–10253.
- (57) Zhang, J.; Xie, R.; Yang, W. *Chem. Mater.* **2011**, *23*, 3357–3361.
- (58) Xiang, W.-D.; Yang, H.-L.; Liang, X.-J.; Zhong, J.-S.; Wang, J.; Luo, L.; Xie, C.-P. *J. Mater. Chem. C* **2013**, *1*, 2014–2020.
- (59) Zhang, W.; Zhong, X. *Inorg. Chem.* **2011**, *50*, 4065–4072.
- (60) Zhong, X.; Feng, Y.; Knoll, W.; Han, M. *J. Am. Chem. Soc.* **2003**, *125*, 13559–13563.
- (61) Zhong, H.; Wang, Z.; Bovero, E.; Lu, Z.; Veggl, F. C. J. M.; Scholes, G. D. *J. Phys. Chem. C* **2011**, *115*, 12396–12402.
- (62) Greenham, N. C.; Peng, X.; Alivisatos, A. P. *Phys. Rev. B* **1996**, *54*, 17628–17637.
- (63) Xie, R.; Rutherford, M.; Peng, X. *J. Am. Chem. Soc.* **2009**, *131*, 5691–5697.
- (64) Zhang, J. *Z. Acc. Chem. Res.* **1997**, *30*, 423–429.
- (65) Sapra, S.; Prakash, A.; Ghangrekar, A.; Periasamy, N.; Sarma, D. *J. Phys. Chem. B* **2005**, *109*, 1663–1668.
- (66) Chamarro, M. A.; Voliotis, V.; Grousson, R.; Lavallard, P.; Gacoin, T.; Counio, G.; Boilot, J. P.; Cases, R. *J. Cryst. Growth.* **1996**, *159*, 853–856.
- (67) Califano, M.; Franceschetti, A.; Zunger, A. *Nano Lett.* **2005**, *5*, 2360–2364.
- (68) Zhang, J.; Zhang, X.; Zhang, J. Y. *J. Phys. Chem. C* **2009**, *113*, 9512–9515.
- (69) Tan, Z.; Zhang, Y.; Xie, C.; Su, H.; Liu, J.; Zhang, C.; Dellas, N.; Mohny, S. E.; Wand, Y.; Wang, J.; Xu, J. *Adv. Mater.* **2011**, *23*, 3553–3558.
- (70) Chen, B.; Zhong, H.; Zhang, W.; Tan, Z.; Li, Y.; Yu, C.; Zhai, T.; Bando, Y.; Yang, S.; Zou, B. *Adv. Funct. Mater.* **2012**, *22*, 2081–2088.